Strong $E1$ transitions in ^{9}Be, ^{11}Be, and ^{13}C

D. J. Millener, J. W. Olness, and E. K. Warburton
Brookhaven National Laboratory, Upton, New York 11973

S. S. Hanna
Stanford University, Stanford, California 94305
(Received 18 April 1983)

The Doppler shift attenuation method has been used to make two measurements of the mean life of the ^{11}Be 320-keV level. The results are 150±30 fs from the ^{9}Be(t,pγ)^{11}Be reaction and 168±17 fs from the ^{3}H(^{9}Be,pγ)^{11}Be reaction. The adopted value of 166±15 fs, from the present and previous measurements, corresponds to an extremely strong $E1$ transition of 0.36±0.03 W.u. The adopted energy of the ground state transition from this and previous measurements is 320.04±0.10 keV. It is shown that the magnitude of this $E1$ transition can be understood on the basis of shell-model calculations only if realistic single-particle wave functions are used. A similar theoretical treatment is given for strong $E1$ transitions in ^{9}Be and ^{13}C.

[NUCLEAR REACTIONS ^{9}Be(t,pγ)^{11}Be, E(t)=1.5—3.3 MeV, ^{3}H(^{9}Be,pγ)^{11}Be, E(^{9}Be)=10—16 MeV; measured DSA; deduced τ(^{11}Be, 320-keV); calculated $B(E1)$, $B(M2)$ from theory and compared to experiment for ^{9}Be, ^{11}Be, ^{13}C.]

I. INTRODUCTION

Electric dipole transitions between bound nuclear levels are almost invariably strongly hindered with respect to single-particle estimates for the well understood reason that most of the $E1$ strength associated with any given level appears in the giant dipole resonance built on that level. Exceptions occur in light nuclei,[1] usually in the case where the level of non-normal parity has dominantly the structure of a single particle weakly coupled to a core state. We consider the transitions of this type in ^{9}Be, ^{11}Be, and ^{13}C shown schematically in Fig. 1. In these cases the non-normal parity states involve mainly an $s_{1/2}$ or $d_{5/2}$ neutron coupled to the 0^{+} ground state of the core. To give an example, the $\frac{1}{2}^{-} \rightarrow \frac{1}{2}^{+}$ transition in ^{11}Be is the strongest known $E1$ transition between bound nuclear levels.

The objectives of this paper are twofold. First, we wish to confirm a previous measurement[2] of, and to provide a more accurate value for, the lifetime of the ^{11}Be $\frac{1}{2}^{-}$ 320-keV level. The fact that an initial calculation[3] of the $E1$ rate, which used harmonic oscillator wave functions to evaluate the single-particle matrix elements, missed the previously measured lifetime by a factor of 30 provided the initial impetus for remeasurement. The calculation used shell-model wave functions which otherwise give a good account of the $A=11$ nuclei. Second, we wish to demonstrate that the experimental $B(E1)$ values in all these cases can be understood on the basis of shell-model calculations if, and only if, the radial single-particle matrix elements are evaluated taking into account the actual binding energies of the single-particle orbits involved in the transition. Calculations using harmonic oscillator wave functions fail to describe the measured $B(E1)$ values, most dramatically in the case of ^{11}Be.

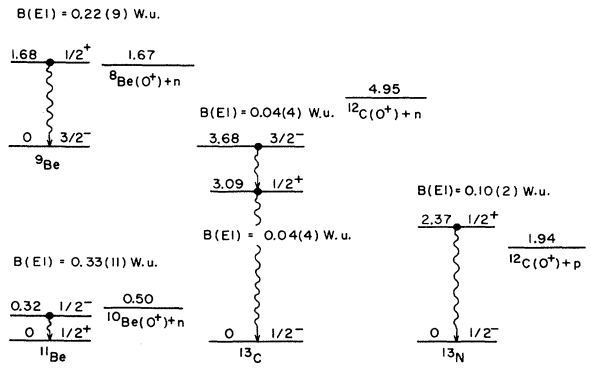

FIG. 1. $E1$ transitions involving $\frac{1}{2}^{+}$ levels in ^{9}Be, ^{11}Be, ^{13}C, and ^{13}N.

II. LIFETIME OF THE ^{11}Be $\frac{1}{2}^{-}$ 320-keV LEVEL

A. General considerations

The previous measurement[2] of the lifetime of the ^{11}Be first-excited state utilized the Doppler shift attenuation method (DSAM). The line shape of the $\frac{1}{2}^{-} \rightarrow \frac{1}{2}^{+}$ 320-keV transition was examined at 0° to the beam in a singles measurement of the ^{9}Be(t,pγ)^{11}Be reaction. Thin ^{9}Be films, 10—20 μg/cm^{2}, both self-supporting and evaporated onto Au, provided line shapes for ^{11}Be recoiling into Au and vacuum, respectively. From these measurements the mean life could be deduced relative to the time scale provided by the stopping time of ^{11}Be ions in Au and Be.

In Sec. II we describe measurements of the lifetime of the ^{11}Be $\frac{1}{2}^{-}$ 320-keV level using the Doppler shift attenuation method (DSAM) applied to the ^{9}Be(t,pγ)^{11}Be and ^{3}H(^{9}Be,pγ)^{11}Be reactions. In Sec. III we present the results of shell-model calculations for ^{9}Be, ^{11}Be, and ^{13}C, concentrating particularly on the evaluation of the single-particle $E1$ matrix elements with Woods-Saxon wave functions.

TABLE I. Parameters for the energy loss of Be ions in Be, Cu, and Au. The parametrization is given in the text.

Stopping material	K_n[a]	K_e	K_3	v_c/v_0	A	B	C	Δ[b]	Range[c] of v/v_0	Norm.[d]	$K_e(LS)$[e]
Au	0.0252	0.320	0.0000					1.78	0.7–1.8	0.978	0.244
Cu	0.0482	0.813	0.0050	2.15	1.183	0.3486	0.0457	1.17	1.1–5.5	0.980	0.641
Be	0.0678	2.525	0.1049	2.30	5.164	−0.2027	0.0258	0.04	1.1–5.5	0.940	2.280

[a]This is the only parameter which depends on the atomic weight of the stopping ion. The numbers are for ^{11}Be.
[b]If a constant uncertainty of Δ is assigned to the tabulation of Ref. 7, then a normalized χ^2 of unity is obtained in the fit to Eq. (1).
[c]The region of v/v_0 included in the fit for ^{11}Be.
[d]The input data is that of Ref. 7 multiplied by Norm. For Cu the input data is that given in Ref. 7 for Ni multiplied by Norm.
[e]The Lindhard-Scharff (Ref. 9) estimate for K_e.

Our first priority was to confirm the previous result. Accordingly, this measurement was repeated with special attention being paid to those aspects where a large systematic error might have occurred. A second priority was to obtain a more accurate value for the mean life, previously measured with a 33% uncertainty. The accuracy of the DSAM applied to the ^{9}Be(t,pγ) ^{11}Be reaction (singles) is limited because the Doppler shift of $\sim$3.5–4 keV is not much larger than the detector resolution ($\sim$1 keV) and the kinematic broadening ($\sim$1.6 keV) due to the (t,p) angular distribution. A factor of 3 in the Doppler shift is gained by inverting the reaction and operating at the same center-of-mass energy. In addition, measurement by both ^{9}Be(t,pγ) and ^{3}H(^{9}Be,pγ) allows a useful check on the consistency of the kinematics and stopping powers involved. Accordingly, a DSAM measurement on ^{3}H(^{9}Be,pγ) ^{11}Be was also undertaken. We next consider the specific energy loss of ^{9}Be ions in ^{9}Be, Au, and Cu necessary to the analysis of the DSAM results.

There is no direct experimental data for the stopping of Be ions in Be, Cu, or Au. The specific energy loss of ^{11}Be in these materials was obtained by interpolation for both incident ions and stopping material. In this interpolation, major reliance was placed on the five effective charge procedures outlined by Warburton, Olness, and Lister.[4] Consideration was also given to the low velocity data presented or reviewed by Warburton, Alburger, and Wilkinson[5] and by Fisher *et al.*[6] The specific energy loss is parametrized by[4]

$$-M\frac{dv_z}{dt}=\frac{-dE}{d(\rho x)}=K_n(v/v_0)^{-1}+K_e(v/v_0)-K_3(v/v_0)^3 \quad (1a)$$

for $0<v<v_c$, and

$$-M\frac{dv_z}{dt}=\frac{-dE}{d(\rho x)}=A+B(v/v_0)-C(v/v_0)^2 \quad (1b)$$

for $v>v_c$. In Eq. (1) v_0 is the Bohr orbital velocity ($c/137$), and ρ is the density of the stopping material; the K_n and K_e terms represent the nuclear and electronic stopping, respectively, while K_3, A, B, C, and v_c are purely phenomenological. The parameters of Eq. (1) are listed in Table I for ^{11}Be stopping in Au, Cu, and Be. The input data for the fits yielding these parameters are essentially those of Northcliffe and Schilling,[7] multiplied by the normalization factor, Norm., of Table I. However, for $v/v_0<1.0$, the parameters of Table I deviate somewhat from this recipe. The nuclear stopping parameter K_n is taken as 1.26 times the Bohr estimate[8] evaluated at $v/v_0=1$. The often-used Lindhard-Scharff estimate[9] for K_e is also given in Table I.

B. The ^{9}Be(t,pγ) ^{11}Be measurement

This reaction was initiated by bombarding thin Be targets with 50–100 nA triton beams from the 3.5-MV Van de Graaff accelerator. Gamma rays were detected by an escape suppression spectrometer (ESS) mounted on a goniometer which could be rotated about the target in the angular range $0°<\theta_\gamma<120°$ with a relative precision of 0.1°. The ESS used a central n-type hyperpure Ge detector, of 20% efficiency with an energy resolution of 2.0 keV at 1332 keV, which was operated in an NaI(Tl) anticoincidence shield described in detail previously.[10]

Two types of targets were used: (1) a 15-μg/cm^2 layer

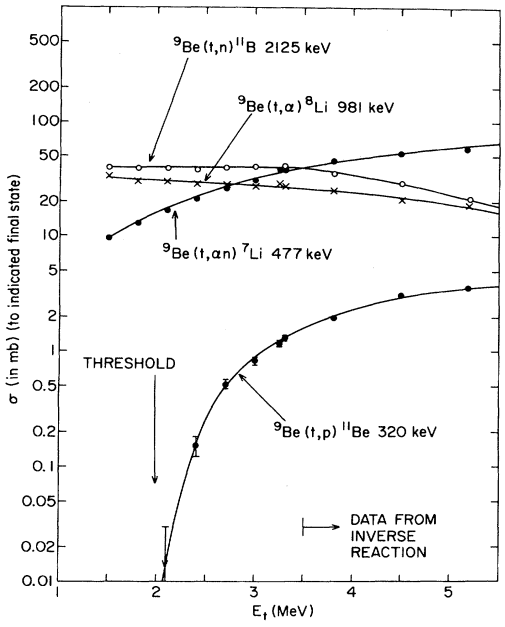

FIG. 2. Yield curves for various reactions induced by triton bombardment of a beryllium target. The absolute cross sections refer to production of the first-excited states of the final nuclei, as measured by observation of the resultant γ-ray deexcitation. Data for $E_t>3.5$ MeV are from the inverse reaction, with appropriate corrections for differing target thicknesses and energy losses.

of Be evaporated onto a 50-μm gold backing, and (2) a 20-μg/cm^2 self-supporting Be target placed in front of a 50-μm gold beam stop. For convenience, we designate the targets as Be-Au and Be-vac, respectively.

Yield curve measurements were made in the range $1.5 < E(t) < 3.3$ MeV using the Be-Au target at a nominal detection angle $\theta_\gamma = 90°$. The efficiency of the ESS as a function of E_γ was determined using sources of ^{133}Ba, ^{137}Cs, ^{152}Eu, and ^{228}Th, which established an absolute calibration over the range 122—2614 keV. The incident triton flux was measured with a standard current integrator. Figure 2 shows the absolute cross sections for production of deexcitation γ rays from the first-excited states of those final nuclei formed most strongly in the triton bombardment. The ^{9}Be(t,p)^{11}Be* ($E_x = 320$ keV) reaction exhibits a clear threshold effect, as expected from the negative Q value[11] for formation of the 320-keV level: $Q = -1.167$ MeV. For comparison, the (t,α), (t,αn), and (t,n) reactions all have positive Q values[11,12] and exhibit markedly different behaviors.

Additional spectra from the reaction were acquired at $\theta_\gamma = 90°$ (nominal) with a ^{133}Ba source placed on the γ-detection axis. The energy calibration was subsequently based on the ^{133}Ba lines[13] at 302.858(5) and 356.014(9) keV as well as on the ^{197}Au 279.01(1)-keV line[13] produced in the Au backing. An energy calibration good to 0.02 keV was established from the data. The mean energy of the ^{11}Be peak was found to be 320.42(4) keV.

However, the observed centroid energy of a Doppler-shifted line is critically dependent on the actual angle of observation θ_γ, as given by the first-order relationship

$$\langle E_\gamma \rangle = E_{\gamma 0}(1 + \langle \beta_z \rangle F(\tau)\cos\theta_\gamma) \ . \quad (2)$$

Here $E_{\gamma 0}$ is the unshifted transition energy, $\langle \beta_z \rangle \equiv \langle v_z/c \rangle$ is the mean z-component velocity (beam axis) of the ensemble of recoil nuclei, and $F(\tau)$ is the attenuation factor which depends on the nuclear lifetime.

Careful measurement of the geometry determined that the nominal 90° data actually corresponded to a mean detection angle of 83.5(7)°. An independent measure of θ_γ was obtained from the observed small shifts of the 478- , 981- , and 2125-keV lines (reactions identified in Fig. 2), with the result $\theta_\gamma = 82.8(8)°$. This latter determination is based on Eq. (2) using previously measured values[11,12] for $E_{\gamma 0}$ as well as the experimental restriction $\tau \lesssim 0.1$ ps, which ensures that $F(\tau) \cong 1$ for all three cases.

The two determinations for θ_γ are in satisfactory agreement, and we adopt the average result $\theta_\gamma = 83.2(7)°$. Using the measured value for $\langle E_\gamma \rangle$ and the product $\beta_z \times F(\tau) = 0.0079$ as determined in the following section, Eq. (2) yields the value

$$E_{\gamma 0} = 320.10(10) \text{ keV} \ .$$

The correction term is necessitated by the fact that $\theta_\gamma \neq 90°$ amounted in this case to $\Delta E = 0.32(4)$ keV. The present result for $E_{\gamma 0}$ is in fair agreement with, but more accurate than, the previous value,[2]

$$E_{\gamma 0} = 319.8(2) \text{ keV} \ .$$

We adopt the weighted average value

$$E_{\gamma 0} = 320.04(10) \text{ keV (adopted value)} \ .$$

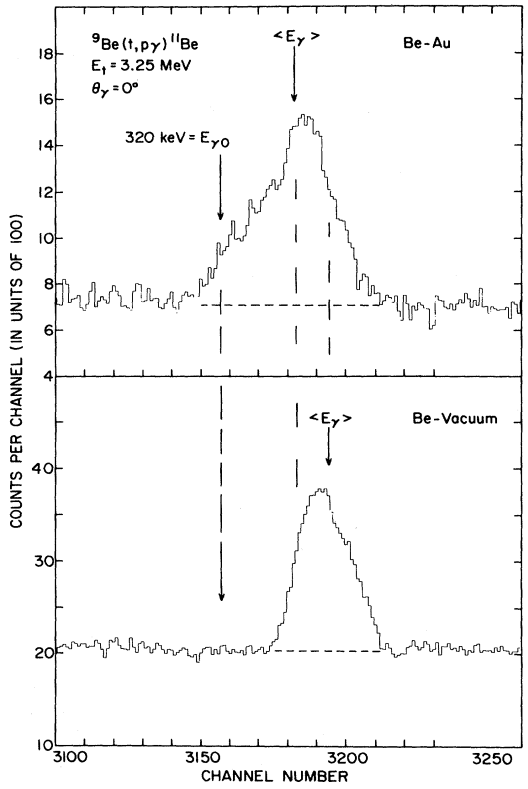

FIG. 3. Line shapes measured at $\theta_\gamma = 0°$ for ^{11}Be nuclei stopping in gold (top) and recoiling into vacuum (bottom). The centroids of the peak distributions are marked by the arrows; the unshifted energy $E_{\gamma 0}$ is also indicated.

Two separate and complete sets of measurements were undertaken at $E(t) = 3.5$ MeV and $\theta_\gamma = 0°$ in order to determine $F(\tau)$: the results are consistent and thus we show the summed data in Fig. 3. Bombardment of the Au backing (i.e., no Be) indicated an essentially featureless "background" spectrum in the region of interest, which was subsequently subtracted from the ^{11}Be spectra. The remaining background was approximated by a first-order polynomial fit to the data above and below the peaks. This background was subtracted from the data before calculating the centroid energies of the Doppler-shifted peaks. The energy calibration, as described above, was based on the ^{133}Ba and ^{197}Au lines. From Eq. (2) the Doppler shift can be calculated as

TABLE II. DSAM data on the ^{11}Be 320→ 0 transition.

θ_γ	Target	$\langle E_\gamma \rangle$ (keV)	$\Delta E_\gamma(0°-90°)$ (keV)	$F(\tau)$
90°	Be-Au	320.04(10)[a]		
0°	Be-Au	322.42(4)	2.39(11)	0.671(36)
0°	Be-vac	323.60(4)	3.56(11)	
0°	Calc.[b]		3.82	

[a]Adopted average value from this work and Ref. 2.
[b]Calculated for ^{9}Be(t,p)^{11}Be* at $E_t = 3.25$ MeV, allowing for triton and ^{11}Be* energy losses in the target layer and assuming an isotropic (t,p) angular distribution in the c.m. system.

$$\Delta E_\gamma = \langle E_\gamma \rangle - E_{\gamma 0} \ . \tag{3}$$

The results, specific to a given target-backing arrangement, are summarized in Table II. The attenuation factor for ^{11}Be nuclei stopping in gold is then easily calculated as

$$F(\tau) = \frac{\Delta E_\gamma(\text{Be-Au})}{\Delta E_\gamma(\text{Be-vac})} \ . \tag{4}$$

This expression is exact for identical ^{9}Be target thicknesses; in the present case, the effect of the small difference is negligible in comparison to the statistical uncertainties.

The asymmetry of the Be-vac data (Fig. 3) indicates clearly that the (t,p) reaction is forward peaked, consistent with the expectation that the $J^\pi = \frac{1}{2}^-$ ^{11}Be state will be formed dominantly by $L=2$ stripping. For the Be-vac case, $F(\tau) \equiv 1$, so that these data define, via Eq. (2), an experimental value for the recoil ^{11}Be nuclei of $\beta_z(\text{expt.}) = 0.0111$. From the kinematics one calculates, for an assumed isotropic (t,p) distribution, $\beta_z(\text{calc.}) = 0.0119$ (see Table II). The experimental value is only 93(2)% of the latter, providing some quantitative measure of the (t,p) anisotropy.

Extraction of a value for the mean life τ from the measured $F(\tau)$ follows the method of Blaugrund.[14] The electronic stopping power was taken as $K_e(v/v_0)$ with the values of K_e for Be stopping in Be and Au given in Table I. The parametrization of the nuclear stopping power due to Oetzmann[15] was used, i.e.,

$$(d\epsilon/d\rho)_n = \frac{1.7\epsilon^{1/2}\ln(\epsilon+e)}{1+6.8\epsilon+3.4\epsilon^{3/2}} \ , \tag{5}$$

where the universal unit of energy ϵ and length ρ are defined by Blaugrund.[14] The result is

$$\tau = 150 \pm 30 \text{ fs} \ .$$

The uncertainty is composed of contributions in quadruture of 15% from the measurement of $F(\tau)$, 12% from K_n, and 15% from K_e.

C. The ^{3}H(^{9}Be,pγ) ^{11}Be reaction

The tritium target for this measurement consisted of 500 μg/cm^2 of Ti on a thick Cu backing, with tritium absorbed into the Ti layer such that there were $\sim$0.75 ^{3}H atoms for each Ti atom. This target was bombarded with ^{9}Be ions from the BNL MP Tandem Facility. Gamma rays were detected with the ESS spectrometer used also in the ^{9}Be(^{3}H,pγ)^{11}Be measurements.

A yield curve was first obtained for $\theta_\gamma = 90°$. These data were combined with those from ^{9}Be(^{3}H,pγ) ^{11}Be to produce the composite curve shown and discussed in Fig. 2.

Next, spectra were recorded at $\theta_\gamma = 0°$ for $E(^9\text{Be}) = 10.5$ and 11 MeV, corresponding to $E(t) = 3.5$ and 3.67 MeV in the inverse reaction. For both spectra the integrated beam current was $\sim$0.2 μC. The only structure in the background underlying the 0° 320-keV line shapes was that due to the Compton backscattering peak from 511-keV radiation, which was easily subtracted. [There was also an unidentified contaminant peak very close to (but less than) 320 keV, but since the 0° 320-keV line shape was confined to higher energies there was no overlap with this contaminant.] The remaining background was approximated by a quadratic function which was fit to the regions above and below the 320-keV line shape. The line shape for $E(^9\text{Be}) = 10.5$ MeV with background subtracted is shown in Fig. 4.

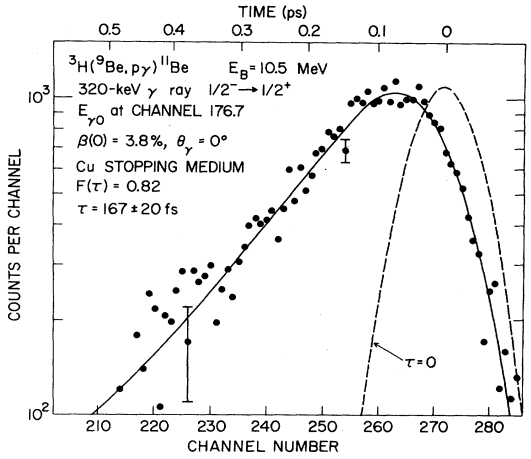

FIG. 4. Line shape observed for the ^{11}Be 320→0 transition following bombardment of a 500 μg/cm^2 ^{3}H-Ti target on a thick Cu backing by 10.5-MeV ^{9}Be ions. The theoretical curve and the extraction of $F(\tau)$ and τ are explained in the text. A prompt ($\tau \simeq 0$) line shape is shown for comparison. The detector response function represented by this curve is a convolution of the detector line shape with kinematical broadening effects due to the spread in the angle and energy of the recoiling ^{11}Be ions. The energy dispersion is 0.132 keV/channel.

The theoretical fit to the line shapes was performed with a program, described previously,[4,16,17] which folds the detector response and kinematical conditions and corrections into a theoretical line shape based on the parametrization of dE/dx given in Eq. (1). The fit to the data shown in Fig. 4 yields a Doppler shift of 12.25(15) keV. This is in close agreement with the kinematical center-of-mass Doppler shift of 12.05 keV calculated for an isotropic distribution. For a forward-peaked distribution of protons in the ^{9}Be(t,p) ^{10}Be reaction, there will be a corresponding forward-peaked distribution of ^{11}Be ions in the inverse ^{3}H(^{9}Be,p) ^{11}Be reaction, and the fractional change of the mean velocity of the ^{11}Be ions from the center-of-mass velocity will be three times as large in ^{9}Be(t,p) and in the opposite direction. Thus, for the observed ratio 12.25/12.05 = 1.0166 from ^{3}H(^{9}Be,p) we predict a mean velocity 95% [i.e., 100 − 3(1.66)] of $\beta_{\text{c.m.}}$ at 3.5 MeV in the ^{9}Be(t,pγ) ^{10}Be reaction. This is in agreement with the previous result[2] for $E(t) = 3.5$ MeV, and also with the result reported in Sec. II B, performed at $E(t) = 3.25$ MeV, which gave $\langle \beta_z \rangle = (93 \pm 2\%)\beta_{\text{c.m.}}$.

Were it not for the spread due to the target thickness, there would be a one-to-one correspondence between channel number (γ energy) and decay time in a γ-ray line shape. This is illustrated by the time scale at the top of Fig. 4 for the *average* recoils, i.e., production of ^{11}Be at the target midpoint. As discussed previously,[16,17] a $\theta_\gamma = 0°$ line shape is clearly similar to a radioactive decay curve with the detector response function (the dashed $\tau = 0$ curve of Fig. 4) analogous to a prompt time resolution function.

The least-squares fit to extract the mean life of the ^{11}Be 320-keV level was done in the same way as above but confined to the energy region corresponding to times after all the ^{11}Be recoils had left the target and entered the Cu backing ($<$ channel 262 in Fig. 4). With this restriction the uncertainty in the target composition had only minimal effect on the final extracted mean life.

The results from the two line shape fits were $\tau=167(20)$ and 170(20) fs for the 10.5 and 11.0 MeV data, respectively. The errors include all known uncertainties except that in dE/dx. Combining the two results and allowing a 5% uncertainty in dE/dx, we obtain

$$\tau=168\pm17 \text{ fs}$$

for the ^{11}Be 320-keV level.

D. Summary of experimental results

The two measurements of the mean life of the ^{11}Be 320-keV level, 150(30) fs from ^{9}Be(t,pγ) and 168(17) fs from ^{3}H(^{9}Be,pγ), are in good agreement with each other and with the previous value[2] of 180(60) fs. The consistency of the three lifetime measurements, along with the identity of the γ ray as confirmed by the yield curves from ^{9}Be(t,pγ) and ^{3}H(^{9}Be,pγ) establish the result beyond a reasonable doubt. We adopt the weighted average of

$$\tau(^{11}\text{Be 320-keV level})=166\pm15 \text{ fs}$$

(adopted value). The adopted value for the lifetime corresponds to a very large $B(E1)$ of 0.36(3) W.u.

III. SHELL-MODEL CALCULATIONS

A. The structure calculation

The wave functions used to calculate electromagnetic matrix elements for ^{9}Be, ^{11}Be, and ^{13}C are obtained from full $0\hbar\omega$ and full $1\hbar\omega$ shell-model calculations for negative- and positive-parity levels, respectively. The Cohen-Kurath interaction[18] is used for the p shell and the Millener-Kurath interaction[19] is used for the p-sd interaction. The calculations for ^{11}Be and ^{13}C have been described previously (Refs. 3 and 20, respectively); the calculation for ^{9}Be differs from these only in that the Cohen-Kurath (6—16) two-body matrix element (TBME) interaction[18] is used in place of the (8—16) TBME interaction.

In earlier work[20] on ^{13}C only harmonic oscillator wave functions (HOWF's) were used and all three $B(E1)$ values for transitions between bound states were underestimated by factors of up to 3. For the ^{11}Be $\frac{1}{2}^{-}\rightarrow\frac{1}{2}^{+}$ transition the use of HOWF's led[3] to an underestimate of the $B(E1)$ by a factor of 30 while the use of Woods-Saxon wave functions (WSWF's) gave[3] a greatly increased $B(E1)$ value. The principal purpose of Sec. III is to consider carefully the use of realistic single-particle wave functions (SPWF's) to compute the single-particle matrix elements (SPME's) which enter into the $E1$ transitions (in one case an $M2$ transition). The $E1$ transitions involving $\frac{1}{2}^{+}$ levels and the relevant particle thresholds are shown in Fig. 1.

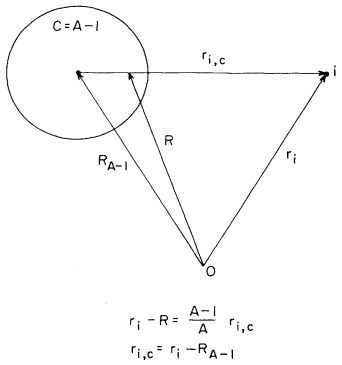

FIG. 5. Coordinate system for an A-particle nucleus.

B. Relative coordinate description

In the standard shell model a many-particle wave function is an antisymmetrized product of single-particle wave functions for each nucleon. When we use the standard shell-model fractional parentage expansion the wave function of the separated particle is a function of the radial coordinate relative to the origin of the potential well (r_i for $i=A$ in Fig. 5). However, the SPWF's obtained by solving the Schrödinger equation with a Woods-Saxon potential are explicitly a function of the relative coordinate between particle and core ($r_{i,c}$ in Fig. 5). Consequently, we require a different fractional parentage expansion in which the wave function of the separated particle is a function of the relative coordinate between the core and the particle. In the harmonic oscillator model it is well known (see, e.g., Ref. 21) that the spectroscopic amplitude appropriate to the relative coordinate description is larger than the standard shell-model spectroscopic amplitude relating physical, i.e., nonspurious, A and $A-1$ particle states by a factor $(A/A-1)^{Q/2}$, where $Q=2n+l$ is the oscillator energy of the separated particle. This means, e.g., that in a p-shell nucleus the effective number of p-shell particles is $(A-4)\times(A/A-1)$ while the number of s-shell particles is $3\times(A/A-1)$; the reduction below 4 in the number of s-shell nucleons is a reflection of the existence of spurious $1\hbar\omega$ shell-model configurations containing s-hole components.

Consider the usual shell-model expression for the matrix elements of a one-body operator O in terms of one-body density matrix elements (OBDME's) and SPME's,

$$\langle J_f T_f M_{T_f}||O||J_i T_i M_{T_i}\rangle=\langle T_i M_{T_i}\Delta T M_{\Delta T}\,|\,T_f M_{T_f}\rangle \times\sum_{j_1 j_2}\frac{\hat{j}_1\hat{\frac{1}{2}}}{\hat{\Delta J}\hat{\Delta T}}\langle j_1\tfrac{1}{2}|||O|||j_2 1/2\rangle\langle J_f T_f|||(a^{\dagger}_{j_1}\tilde{a}_{j_2})^{\Delta J\Delta T}|||J_i T_i\rangle\,, \tag{6}$$

where ΔJ and ΔT are the space-spin and isospin ranks of the operator O. Equation (6) is obtained under the assumption

that the wave functions of neutrons and protons are the same and do not depend on the core configuration to which they are coupled. To take binding energies into account, a step back in the derivation of Eq. (6) is made to obtain

$$\langle J_f T_f M_{T_f}||O||J_i T_i M_{T_i}\rangle$$
$$=(-)^{j_1+j_2-\Delta J}\sum_{\alpha_c J_c T_c j_1 j_2} U(J_f j_1 J_i j_2, J_c \Delta J)\langle J_f T_f|||a^\dagger_{j_1}|||\alpha_c J_c T_c\rangle(-)^{T_c+1/2-T_i}\frac{\hat{T}_c}{\hat{T}_i}\langle \alpha_c J_c T_c|||\tilde{a}_{j_2}|||J_i T_i\rangle$$
$$\times\sum_{m_t(m_t' M_{T_c})}\langle T_c M_{T_c}\tfrac{1}{2}m_t \mid T_f M_{T_f}\rangle\langle T_c M_{T_c}\tfrac{1}{2}m_t' \mid T_i M_{T_i}\rangle\frac{\hat{j}_1}{\hat{\Delta J}}\langle j_1\tfrac{1}{2}m_t||0||j_2\tfrac{1}{2}m_t'\rangle\ . \tag{7}$$

Particle coordinates are usually used in Eq. (6) in which case the core-state sum, implicit in Eq. (6) and explicit in Eq. (7), goes over all shell-model configurations, spurious and nonspurious; in this case HOWF's are functions of r_A/b_0 where b_0 is the oscillator length parameter. To work with relative coordinates the core-state sum in Eq. (7) must be restricted to nonspurious configurations and factors $(A/A-1)^{Q_1/2}$ and $(A/A-1)^{Q_2/2}$ must multiply the normal shell-model spectroscopic amplitudes; for HOWF's the appropriate length parameter would then be $b_{\rm rel}=(A/A-1)^{1/2}b_0$. For WSWF's Eq. (7) is used with $\alpha_c J_c T_c$ labeling physical core states and the separation energies dependent on the specific core state. This is but a prescription, albeit reasonable in that the SPWF's have the correct asymptotic form, similar to that normally used to analyze single-particle transfer reactions.

C. Choice of Woods-Saxon parameters

We fix the radius parameter, $R=r_0(A-1)^{1/3}$, of the Woods-Saxon well so that the r.m.s. charge radii of ^{9}Be, ^{11}B, and ^{13}C, computed using Cohen and Kurath's p-shell spectroscopic amplitudes,[22] fall within the range specified by elastic electron scattering and muonic x-ray data; the diffuseness parameter we fix at $a_0=0.65$ fm and we set the spin-orbit potential to zero.

To calculate r.m.s. radii we write

$$\sum_i(\vec{r}_i-\vec{R})^2=\left[\frac{A-1}{A}\right]^2\sum_i\vec{r}_{i,c}^{\,2} \tag{8}$$
$$=\sum_i\vec{r}_i^{\,2}-A\vec{R}^{\,2}\ , \tag{9}$$

TABLE III. Root-mean-square charge radii.

Nucleus	b_0 (fm)[a]	HO	$\langle r^2\rangle_{\rm ch}^{1/2}$ (fm) Expt.[b]	WS[c]	r_0 (fm)
^{13}C	1.684	2.54	2.45–2.51	2.47	1.4
^{12}C	1.669	2.52	2.45–2.47	2.46	1.4
^{11}B	1.653	2.45	2.42–2.47	2.39	1.4
				2.45	1.47
^{9}Be	1.617	2.33	2.46–2.52	2.28	1.5
				2.35	1.6
				2.46	1.75

[a] $b_0^2=41.467/\hbar\omega$, $\hbar\omega=45A^{-1/3}-25A^{-2/3}$ (Ref. 24).
[b] Taken from the tabulations by Ajzenberg-Selove (Refs. 11, 12, and 25 and references therein). A recent analysis (Ref. 26) of muonic x-ray data gives $\langle r^2\rangle_{\rm ch}^{1/2}=2.47\pm0.02$ (^{12}C) and 2.48 ± 0.02 (^{13}C).
[c] $a_0=0.65$ fm, $r_c=1.6$ fm, $V_{\rm SO}=0$.

where $\vec{r}_{i,c}$ is the core-particle relative coordinate and $\vec{R}$ is the center-of-mass coordinate of the A particle nucleus (Fig. 5). When HOWF's are used, Eq. (8) in the relative coordinate description and Eq. (9) in the particle coordinate description give the same results. For the charge radius Eq. (8) gives

$$\langle r^2\rangle_{\rm ch}=\frac{1}{Z}\left[\frac{A-1}{A}\right]^2\left[\left[2-\frac{Z-2}{A-1}\right]\langle r^2\rangle_s + \sum_c C^2S(c)\langle r^2\rangle_{\rm pc}\right]+\langle r^2\rangle_{\rm pr}\ , \tag{10}$$

where the last term refers to the charge radius of the proton (we take $\langle r^2\rangle_{\rm pr}=0.64$ fm^2), and

$$\sum_c C^2S(c)=\frac{A}{A-1}(Z-2)\ . \tag{11}$$

In our calculations we bind the $0s$ proton at 32–34 MeV as suggested by (p,2p) experiments.[23] In the p-shell contribution the $S(c)$ are the Cohen and Kurath spectroscopic factors[21] for each parent, denoted by c, and $\langle r^2\rangle_{\rm pc}$ is the expectation value of $r_{i,c}^2$ computed for the separation energy corresponding to that parent.

The calculated r.m.s. charge radii are given in Table III, on the basis of which we choose $r_0=1.4$, 1.47, and 1.75 fm to calculate SPME's for ^{13}C, ^{11}Be, and ^{9}Be, respectively. The SPME's for $E1$ and $M2$ transitions vary only slowly with r_0 so that the choice of r_0 is not particularly critical; for HOWF's the SPME's vary linearly with b_0 and hence very nearly linearly with $\langle r^2\rangle_{\rm ch}^{1/2}$. The $E1$ operator expressed in relative coordinates is

$$O(E1)=e/2\sum_i(\vec{r}_i-\vec{R})\tau_{3i}$$
$$=\frac{A-1}{A}\frac{e}{2}\sum_i r_{i,c}\tau_{3i}\ . \tag{12}$$

D. The ^{11}Be $\frac{1}{2}^-\rightarrow\frac{1}{2}^+$ transition

This transition has already been briefly discussed in a paper[3] on the β decay of ^{11}Be. In Table VI of Ref. 3 the OBDME's appropriate to the particle description are listed, as are the SPME's calculated with HOWF's. A complete breakdown of the computation of the $E1$ matrix element in the relative coordinate scheme is given in Table IV. The enormous increase, by a factor of 50, in the $B(E1)$ for $r_0=1.47$ fm over the HO value can be mainly

TABLE IV. $\frac{1}{2}^- \rightarrow \frac{1}{2}^+$ $E1$ transition in ^{11}Be.

Orbits[a] $j_1 j_2$	BE (MeV)[b] j_1	j_2	J_c^π	OBDME[c]	SPME[d] WS ($r_0=1.47$)	WS ($r_0=1.2$)	HO[e]
$1s_{1/2}p_{1/2}$	0.50	0.18	0_1^+	−0.8992	−2.312	−2.202	−0.743
	11.06	10.74	0_2^+	−0.0353	−0.951	−0.908	
$d_{5/2}p_{3/2}$	3.87	3.55	2_1^+	−0.2393	2.699	2.445	2.229
	6.46	6.14	2_2^+	0.0140	2.518	2.277	
	9.77	9.45	2_3^+	−0.0124	2.373	2.144	
	10.37	10.05	2_4^+	−0.0164	2.353	2.124	
$1s_{1/2}p_{3/2}$	8.99	8.67	1_1^+	−0.0725	−1.419	−1.356	−1.051
$d_{3/2}p_{3/2}$	3.87	3.55	2_1^+	−0.0440	−0.900	−0.815	−0.743
	6.46	6.14	2_2^+	0.0122	−0.839	−0.759	
	8.99	8.67	1_1^+	0.0215	−0.801	−0.724	
$p_{1/2}0s_{1/2}$	21.8	21.5		0.0276	−0.958	−0.863	−0.910
$p_{3/2}0s_{1/2}$	21.8	21.5		0.0298	1.355	1.220	1.287
Σ SPME×OBDME$=M$					1.563	1.519	0.245
$B(E1)$ W.u.[f]					0.55	0.52	0.011
$\langle r^2\rangle_{ch}^{1/2}$					2.45	2.25	2.45

[a]The $d_{3/2}p_{1/2}$ contribution is negligible.
[b]Binding energy of single-particle orbit in MeV.
[c]Small contributions from higher core states are included in the highest energy core state listed.
[d]$\langle j_1||0||j_2\rangle \hat{j}_1/\Delta\hat{J}$ for $0=\vec{r}-\vec{R}=\frac{10}{11}\vec{r}_{i,c}$.
[e]$b_0=1.6528$ fm (see Table III).
[f]$B(E1)=(3/4\pi)\frac{3}{10}M^2e^2$ fm^2, W.u.$=(1/4\pi)(\frac{3}{4})^2(1.2A^{1/3})^2=0.3188e^2$ fm^2 for $A=11$.

attributed to the large increase in the $1s_{1/2}p_{1/2}$ SPME for neutrons loosely bound to the ground state of the ^{10}Be core. Particularly significant is the increase in the $1s_{1/2}p_{1/2}$ SPME relative to the $d_{5/2}p_{3/2}$ SPME, where the particles are coupled to higher core states with correspondingly larger separation energies. The near cancellation of the $1s_{1/2}p_{1/2}$ and $d_{5/2}p_{3/2}$ contributions in the HO calculation is thus removed. We note that to obtain the $1s_{1/2}p_{1/2}$ matrix element for low binding energies it is necessary to integrate out to large radii (35 fm to get the numbers in Table IV); the $B(E1)$ value of 0.21 W.u. given in Ref. 3 is inexact because the range of integration was not large enough. The $B(E1)$ is relatively insensitive to changes in r_0 since the $1s_{1/2}p_{1/2}$ SPME for very loosely bound orbits is less sensitive to the size of the well than the SPME for deeply bound orbits (see Table IV). Thus the use of the proton well geometry to compute the wave functions of loosely bound neutrons should not introduce any significant error into the calculated $B(E1)$.

The $B(E1)$ calculated using WSWF's ($r_0=1.47$ fm) is actually larger than the experimental value of 0.36(3) W.u. by about 50%. While we consider the agreement between theory and experiment to be good, it would be improved if there were a larger $d_{5/2}$ component in the ^{11}Be ground state wave function; if so there would also be improved agreement between theory and experiment for the β decay

TABLE V. $\frac{1}{2}^+ \rightarrow \frac{3}{2}^-$ transition in ^{9}Be.

Orbits		$1s_{1/2}p_{1/2}$	$d_{3/2}p_{1/2}$	$1s_{1/2}p_{3/2}$	$d_{3/2}p_{3/2}$	$d_{5/2}p_{3/2}$	$p_{1/2}0s_{1/2}$	$p_{3/2}0s_{1/2}$	BE $(1s_{1/2})$[a] (MeV)	M	$B(E1)\times10^{-1}$ W.u.
OBDME[a]		0.0028	−0.0642	−1.1395	0.1686	−0.1782	−0.0482	0.0248			
SPME[a]:	HO[b]	−0.719	1.607	−1.016	−0.719	2.156	−0.880	1.245		0.621	0.55
	WS	−0.842	2.070	−2.224	−0.926	2.777	−0.931	1.316	0.5	1.826	4.76
				−2.140					0.2	1.730	4.27
				−2.037					0.1	1.613	3.71
				−1.933					0.05	1.494	3.19
				−1.814					0.02	1.358	2.63
										Expt.	2.2±0.9

[a]See the footnotes to Table IV.
[b]$b_0=1.617$ fm (see Table III). If b_0 is increased to give the same r.m.s. charge radius as the WS ($r_0=1.75$ fm) calculation the $B(E1)$ increases to 0.061 W.u.

TABLE VI. Transitions in ^{13}C.

Orbits		$1s_{1/2}p_{1/2}$	$d_{3/2}p_{1/2}$	$1s_{1/2}p_{3/2}$	$d_{3/2}p_{3/2}$	$d_{5/2}p_{3/2}$	$p_{1/2}0s_{1/2}$	$p_{3/2}0s_{1/2}$	M	$B(L)\times10^{-2}$ W.u.[a]
OBDME[b]: $\frac{1}{2}^+\rightarrow\frac{1}{2}^-$		−1.2869	0.0025	0.0196	−0.0366	−0.2030	0.0282	−0.0173		
SPME[b]:	WS	−1.174	1.663	−1.196	−0.823	2.470	−0.919	1.300	0.971	10.5
	HO[c]	−0.763	1.706	−1.079	−0.763	2.289	−0.934	1.321	0.479	2.6
									Expt.[d]	3.9(4)
OBDME: $\frac{1}{2}^+\leftarrow\frac{3}{2}^-$		−0.0134	−0.0642	−0.6642	0.0298	−0.484	−0.0408	−0.0194		
SPME:	WS	−0.904	1.927	−2.259	−0.862	2.285	−0.919	1.300	1.250	8.7
	HO								0.496	1.4
									Expt.[d]	4.0(4)
OBDME: $\frac{5}{2}^+\rightarrow\frac{3}{2}^-$		−0.1542	0.1027	−0.0282	0.0492	−0.3728(0$^+$)[e] 0.1440(2$^+$)	0.0030	0.0172		
SPME:	WS	−1.132	1.942	−1.277	−0.764	3.138(0$^+$) 2.605(2$^+$)	−0.919	1.300		
									−0.403	1.8
	HO								−0.218	0.53
									Expt.[d]	1.06(5)
		$d_{5/2}p_{1/2}$								
OBDME[f]: $\frac{5}{2}^+\rightarrow\frac{1}{2}^-$		−0.8896	0.0027	0.1294	−0.1077	−0.2913		−0.0492		
SPME:	WS	−2.486	−0.408	−1.716	0.906	2.076		1.592	1.208	95
	HO	−2.047	−0.418	−1.321	0.836	1.915		1.618	0.922	55
									Expt.[d]	47(2)

[a] $B(L)=B(E1)$ or $B(M2)$.
[b] See the footnotes to Table IV.
[c] $b_0=1.6844$ fm.
[d] Reference 20.
[e] The ^{12}C core state for each contribution is given in parentheses.
[f] Almost a pure neutron transition; orbital contribution ≈0 and the isoscalar spin matrix element scales with the dominant isovector spin matrix element.

of ^{11}Be and the $E1$ decays of the ^{11}B analog of the ^{11}Be ground state (see Table VI of Ref. 3).

E. The ^{9}Be $\frac{1}{2}^+\rightarrow\frac{3}{2}^-$ transition

The radiative width of the 1.68-MeV $\frac{1}{2}^+$ level of ^{9}Be has been measured[27] by inelastic electron scattering. Since the separation energy for a neutron is 1.665 MeV, the $\frac{1}{2}^+$ level is slightly unbound. For the purposes of this paper we treat the $\frac{1}{2}^+$ level as bound and study the $1s_{1/2}p_{3/2}$ contribution to the $E1$ matrix element as a function of the binding energy of the $1s_{1/2}$ neutron. The OBDME's and SPME's are given in Table V. For each OBDME the particles are assumed to be bound to the lowest possible core state; in fact, the only important core states are the lowest 0^+ and 2^+ $T=0$ levels. The $1s_{1/2}p_{3/2}$ SPME, and the resultant $B(E1)$, are given for a range of $1s_{1/2}$ binding energies. The WS calculation gives a considerable enhancement of the $B(E1)$ over the HO calculation for reasons similar to those which apply to the ^{11}Be transition; since the experimental transition rate is relatively imprecise and the unbound nature of the $\frac{1}{2}^+$ level is not properly treated in our calculation we do not dwell further on the ^{9}Be $\frac{1}{2}^+\rightarrow\frac{3}{2}^-$ transition.

F. Transitions in ^{13}C

The $E1$ and $M2$ transitions between the bound levels of ^{13}C have been discussed previously.[20] With HOWF's all three $E1$ transition strengths are underestimated by factors of up to 3, whereas the $M2$ transition strength is quite well reproduced. With WSWF's all the transition strengths are overestimated by about a factor of 2 as shown in Table VI. In each case most of the difference between the HO and WS results comes about from the increase in the SPME's associated with the dominant OBDME's where the ^{12}C ground state is the major parent, i.e., $1s_{1/2}p_{1/2}$, $1s_{1/2}p_{3/2}$, $d_{5/2}p_{3/2}$, and $d_{5/2}p_{1/2}$ for the $\frac{1}{2}^+\rightarrow\frac{1}{2}^-$, $\frac{3}{2}^-\rightarrow\frac{1}{2}^+$, $\frac{5}{2}^+\rightarrow\frac{3}{2}^-$, and $\frac{5}{2}^+\rightarrow\frac{1}{2}^-$ transitions, respectively.

We do not attempt to discuss the corresponding transitions in ^{13}N (Fig. 1) since the excited levels are unbound with respect to proton emission; we refer the reader to the comprehensive treatment by Barker and Ferdous.[28]

G. Summary

It is clear from Tables IV—VI that, as one would expect, the single-particle matrix elements for loosely bound particles are considerably larger than those calculated with HO wave functions, particularly if the $1s_{1/2}$ orbit is involved. The increases in the transition matrix elements from this effect are amplified by changes in the cancellation between $p \rightarrow 1s$ and $p \rightarrow d$ contributions. Since the HO calculations give matrix elements that are too small compared to experiment, such increases are welcome, particularly in ^{11}Be, where the very small separation energies for both the p and $1s$ orbitals lead to the largest effect.

The matrix elements with WS wave functions are consistently larger than the experimental values. Since the matrix elements are very sensitive to small changes in the $1s_{1/2}$ and $d_{5/2}$ content of the positive-parity wave functions, the overestimates could be due simply to a deficiency in the structure calculation. However, shell-model configurations higher than $1\hbar\omega$ should also be considered, as should effects of the continuum.

Finally, we emphasize that while the procedure of using a different separation energy for each core state is but a prescription, and cannot be strictly correct, it nevertheless clearly represents a physical effect. The transitions studied in this paper are excellent examples in which to look for such effects since the $E1$ matrix element receives two large contributions of $p \rightarrow 1s$ and $p \rightarrow d$ character. The resultant matrix element is reduced by a cancellation between these two contributions. In contrast, if a matrix element is small because all contributions from different pairs of orbits are individually small the choice of the single-particle wave function is essentially irrelevant.

We conclude that care must always be taken to use realistic single-particle wave functions in the calculation of $E1$, $M2$, and related matrix elements which enter into the description of first-forbidden β decay and parity nonconservation in nuclei; such care is necessary before any statement can be made about the presence of meson exchange-current contributions in nuclear matrix elements.

This work was supported by U.S. Department of Energy Contract DE-AC02-76CH00016 and the National Science Foundation.

[1]P. M. Endt, At. Data Nucl. Data Tables 23, 3 (1979).
[2]S. S. Hanna, K. Nagatani, W. R. Harris, and J. W. Olness, Phys. Rev. C 3, 2198 (1971).
[3]D. J. Millener, D. E. Alburger, E. K. Warburton, and D. H. Wilkinson, Phys. Rev. C 26, 1167 (1982).
[4]E. K. Warburton, J. W. Olness, and C. J. Lister, Phys. Rev. C 20, 619 (1979).
[5]E. K. Warburton, D. E. Alburger, and D. H. Wilkinson, Phys. Rev. 129, 2180 (1963).
[6]T. R. Fisher, S. S. Hanna, D. C. Healey, and P. Paul, Phys. Rev. 176, 1130 (1968).
[7]L. C. Northcliffe and R. F. Schilling, Nucl. Data A7, 233 (1970).
[8]N. Bohr, K. Dan. Vidensk. Selsk, Mat.—Fys. Medd. 18, No. 8 (1948).
[9]J. Lindhard and M. Scharff, Phys. Rev. 124, 128 (1961).
[10]J. Konijn, P. F. A. Goudsmit, and E. W. A. Lingeman, Nucl. Instrum. Methods 109, 83 (1973).
[11]F. Ajzenberg-Selove and C. L. Busch, Nucl. Phys. A336, 1 (1980).
[12]F. Ajzenberg-Selove, Nucl. Phys. A320, 1 (1979).
[13]*Tables of Isotopes,* 7th ed., edited by C. M. Lederer and V. S. Shirley (Wiley, New York, 1978).
[14]A. E. Blaugrund, Nucl. Phys. 88, 501 (1966).
[15]H. Oetzmann, inaugural dissertation, University of Heidelberg, 1976.
[16]E. K. Warburton, J. W. Olness, G. A. P. Engelbertink, and T. K. Alexander, Phys. Rev. C 7, 1120 (1973).
[17]E. K. Warburton, P. Gorodetzky, and J. A. Becker, Phys. Rev. C 8, 418 (1973).
[18]S. Cohen and D. Kurath, Nucl. Phys. 73, 1 (1965).
[19]D. J. Millener and D. Kurath, Nucl. Phys. A255, 315 (1975).
[20]E. K. Warburton, D. E. Alburger, and D. J. Millener, Phys. Rev. C 22, 2330 (1980).
[21]M. Ichimura, A. Arima, E. C. Halbert, and T. Terasawa, Nucl. Phys. A204, 225 (1973).
[22]S. Cohen and D. Kurath, Nucl. Phys. A101, 1 (1967).
[23]H. Tyrén, S. Kullander, O. Sundberg, R. Ramachandran, P. Isacsson, and T. Berggren, Nucl. Phys. 79, 321 (1966).
[24]J. Blomqvist and A. Molinari, Nucl. Phys. A106, 545 (1968).
[25]F. Ajzenberg-Selove, Nucl. Phys. A360, 1 (1981).
[26]L. A. Schaller, L. Schellenberg, T. Q. Phan, G. Piller, A. Ruetschi, and H. Schneuwly, Nucl. Phys. A379, 523 (1982).
[27]H.-G. Clerc, K. J. Wetzel, and E. Spamer, Nucl. Phys. A120, 441 (1968).
[28]F. C. Barker and N. Ferdous, Aust. J. Phys. 33, 691 (1980).